Towards Reliability-Based Geometry Optimization of a Point-Absorber with PTO Reliability Objectives

Caitlyn E. Clark, Anna Garcia-Teruel, Bryony DuPont, and David Forehand

***Abstract*—In this study, we seek to understand the relationship between wave energy converter (WEC) hull geometries and power take-off (PTO) reliability. To do this, we calculate the damage equivalent loads (DELs) for a PTO given three hull shapes (a cylinder, sphere, and barge), two sets of metocean conditions (from the center of the North Sea and off the west coast of Norway), and two float motions (heave and surge). Results indicate that hull geometry has a primary influence on DELs experienced by the PTO, and also that certain geometries result in larger variations in DELs based on the whether the device is moving in heave or surge motion. These findings underline the importance of considering WEC hull geometry in early design processes to optimize cost, power production, and reliability. More importantly, this research emphasizes the need to consider the relationship between the WEC geometry and the PTO reliability early in the design process. By considering this relationship, more optimal WECs can be designed for power production and system reliability. The methods tested in this study will enable the future reliability-based geometry optimization of WEC hulls to maximize reliability and power production.**

***Index Terms*—reliability-based design, PTO, wave energy, point absorber**

I. Introduction

As the wave energy industry progresses towards commercialization, research and development efforts to characterize and improve reliability of wave energy converters (WECs) have increased. Issues with reliability and survivability of WEC designs have previously led to setbacks for private developers including closure and delayed or limited testing of devices [1]. Moreover, component or system failure rates directly affect capital costs, operational costs, and power production. Therefore, designing WECs to withstand highly energetic wave conditions without over-engineering them is critical to overcoming industrial and development challenges and enable their implementation.

Despite the importance of considering WEC reliability in early design phases, it is often considered secondary to power production. Maximizing power production across sea states can increase revenue potential, but also loads and costs. Thus, there is a design trade-off between power production and component reliability that should be considered throughout the WEC design process. Particularly in device geometry design, there is an opportunity to reduce structural and PTO loads [1]. Optimizing WEC shape for reliability and power could decrease downtime and required maintenance costs. Ensuring that WECs perform as they were designed for their intended lifespan, while decreasing levelized costs of energy, is integral to improving their feasibility.

Previous work pertaining to this research area include 1) WEC hull geometry optimization for cost and power production, 2) reliability-based design optimization of WEC foundations, and 3) WEC hull geometry effects on varying component loads.

First, WEC hull geometries have been optimized for cost and power production, where costs varied with device size. [2]–[4]. In these studies, reliability was not considered. Second, when reliability was incorporated into WEC design optimization, Ambuhl et al. maximized profitability by optimizing foundation diameter and thickness for the WaveStar device given pile failure constraints. The WEC hull shape was not considered [5].

Lastly, a few studies have provided insight into the geometry-dependent structural integrity of WECs. Beirao et al. compared three geometries (a sphere, a horizontal cylinder, and a vertical cylinder with a conical bottom) for a heaving buoy of a point absorber and their effect on component loads. Using Finite Element Methods (FEM), they considered loads on the supporting cables and PTO cylinder rod [6]. They found that, compared to a fully submerged buoy or a buoy floating at the surface, a partially submerged buoy experienced the greatest stresses and excursion. When the piston was retracted the highest loads were observed in the cables, whereas in extended position both rod and cables were identified as critical components. The sphere showed the lowest stress values in both cases. More relevant to the present study, Van Rij et al. compared the resulting PTO DELs from two point absorber floater geometries (a vertical cylinder with truncated conical bottom and a rhombus) and two mooring configurations (a monopile and a spar-plat configuration) [7]. Using CFD to obtain viscous drag coefficients for the WECs, Van Rij et al. generated

This work was supported by the INORE Blue Energy Collaborative Scholarship (inore.org)

C.E. Clark and B. DuPont are affiliated with the School of Mechanical, Industrial, and Manufacturing Engineering and the Pacific Marine Energy Center at Oregon State University, Corvallis, OR 97331 USA (e-mails: clarkc@oregonstate.edu, bryony.dupont@oregonstate.edu).

A. Garcia-Teruel and D. Forehand are with the School of Engineering and the Institute for Energy Systems at The University of Edinburgh, Edinburgh EH9 3BF, UK (emails: a.garcia-teruel@ed.ac.uk, d.forehand@ed.ac.uk)

PTO force data from the time domain model in WEC-Sim. The rhombus float with a spar-plate configuration resulted in the lowest fatigue loads. These two studies inform our understanding of how WEC geometry relates to various component reliability, but both analyses used are too computationally demanding to be used within an optimization process.

This previous literature has enabled the current work, which addresses the opportunity to implement reliability-based design optimization of hull geometries to design more optimal WECs. This would allow for hull geometries with advantageous reliability scores to be prioritized, balancing cost, power production, and reliability objectives. However, to develop this optimization approach, we first need to develop analysis methods that relate environmental loads the WEC experiences to its reliability, as well as evaluate the sensitivity of its reliability to varying hull geometries. In this study, we will explore the relationship between WEC floater geometry and Power Take-Off (PTO) reliability, focusing on developing an assessment method to evaluate PTO damage.

To complete this analysis, we leverage previous work that generates WEC hull geometries and performs hydrodynamic analysis, from which power production and PTO forces for each geometry can be obtained [2], [8]. From this PTO force time series, we use Rainflow Counting and appropriate S-N Curves to count the number of fatigue cycles and relate it to Damage Equivalent Load (DEL) metrics. Investigating various WEC hull geometries will allow us to evaluate and compare several hull shapes and their resulting PTO damage. This study will provide insight about how hull geometries affect PTO damage, and enable future work incorporating this reliability assessment method within a geometry optimization process.

This study is divided into three sections. First, the methodology is described in Section II, which 1) defines the case studies, met-ocean conditions, and WEC system characteristics, 2) describes the hydrodynamic model used to determine the PTO force time series for each case, and 3) details how we calculated the fatigue DELs based on that PTO force time series. The results for all the cases are presented in Section III, with a discussion of those results, the conclusions we can make, and planned future work following in Section IV.

II. Methodology

To investigate the effect of WEC hull geometries on PTO DELs, we consider three different floater shapes, two energy absorption modes, and two geographic locations. We introduce the met-ocean conditions and the main characteristics of the WEC-system in Subsection II-A. Subsection II-B details the hydrodynamic model used to generate the PTO force time series. Concluding, Subsection II-C describes our fatigue analysis methods.

A. WEC system definition

In this study, we analyze a point absorber type WEC oscillating in a single mode of motion (either heave, or surge). The WEC floater reacts against a PTO, such as a linear generator or a hydraulic piston, fixed 1) perpendicular to the sea bed, or 2) perpendicular to some vertical surface in the water column (see Figure 1). We assume the PTO system is composed of a moving rod welded to the floating body and a fixed component. Three different floater shapes were considered: a sphere, a barge, and a cylinder. We chose the dimensions of the three shapes so that their draft and characteristic width would be equivalent. These dimensions are also shown in Figure 1.

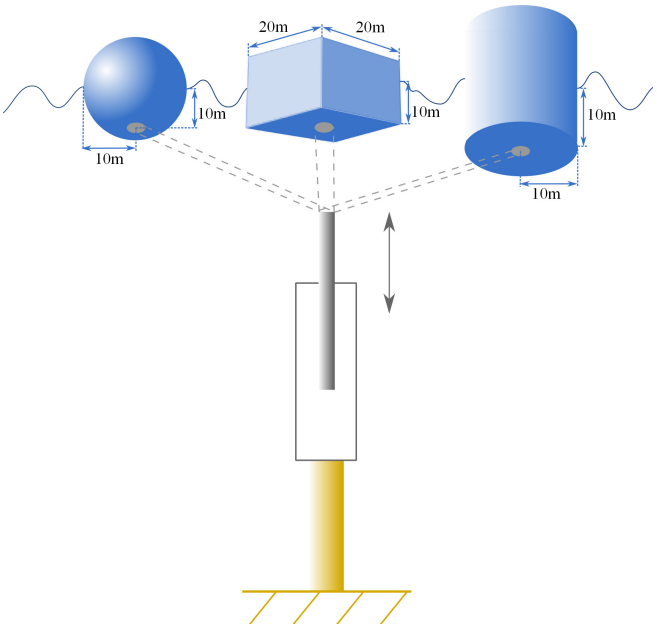

(a) Heave

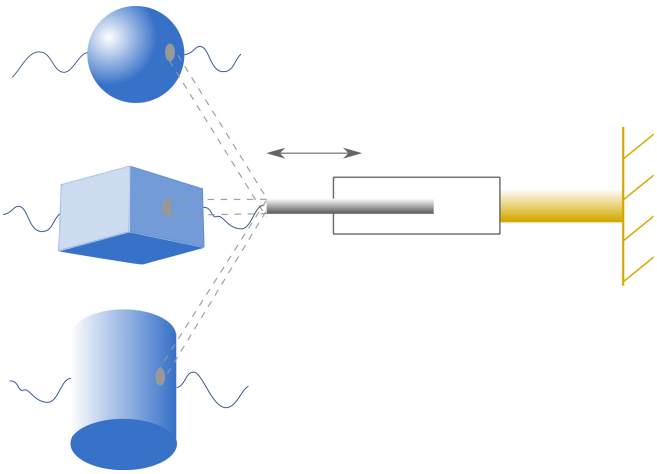

(b) Surge

Fig. 1. Schematic representation of the WEC systems oscillating in (a) heave and (b) surge.

B. Hydrodynamic Modelling

To model the sea states of the two locations, we first derived the characteristic sea states at each location, and then used the resulting H_s, T_p, and probability of occurrence as input for the WEC hydrodynamic model.

1) Study Areas and Sea State Conditions: To model the hydrodynamics of this system, we considered two geographic locations, each with their own set of characteristic sea states. We considered sea states 1) in the

central North Sea and 2) off the southwestern coast of Norway (Figure 2). These two locations correspond to Site 15 and Site 14 (respectively) of the European Union's MARINA Project (or Marine Renewable Integrated Application Platform) [9], and were chosen for the availability of metocean data, as well as because their site conditions are distinct enough to compare WEC response dependence on location. For instance, the sites differ significantly in the average depth at the site, the level of protection from open ocean conditions, and the shape of the sea state conditions distribution. These site conditions are described in Table I.

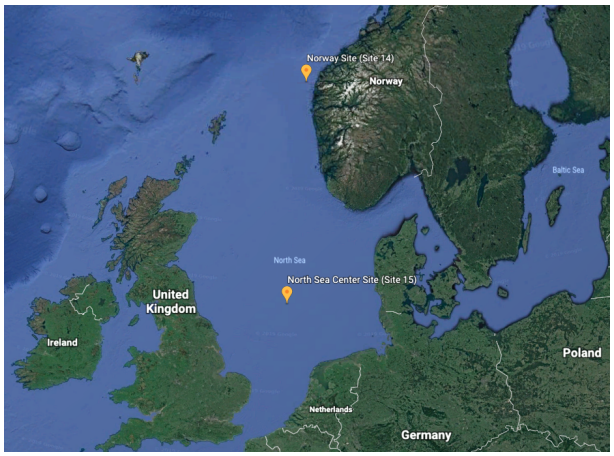

Fig. 2. Site Locations: North Sea Center and Norway

TABLE I
SITE CHARACTERISTICS

	North Sea	Norway
Location	55.13N, 3.43E	61.85N, 4.23E
Water Depth (m)	29	200
Distance to shore (km)	300	30
50-year U_w at 10 m (m/s)	27.2	33.49
50-year H_s (m)	8.66	10.96
Mean value of T_p (s)	6.93	11.06

The MARINA Project provides marginal and joint distributions of wind and wave data for the study locations. The National and Kapodistrian University of Athens provided the 10 years (2001-2010) hourly raw data for the selected offshore sites. Both marginal and joint distributions are obtained by fitting analytic solutions to raw data and are characterized by one-hour mean wind speed at 10 m above mean sea level (U_w), significant wave height (H_s) and spectral peak period (T_p) [10].

The joint probability density function (PDF) of U_w, H_s, and T_p is defined by the marginal PDF of $U_w(fU_w)$, a PDF of H_s conditional on U_w ($fH_s|U_w$) and a PDF of T_p conditional on H_s ($fT_p|H_s$). The parameters and equations that define these distributions can be found in the original description of site conditions [10]. The resulting representative sea states are described in Table II and III. For the purposes of this study, we assume the waves are unidirectional, approaching the WEC from the west.

2) PTO Force estimation: To estimate the PTO force, the WEC motion at each location was analysed with a

TABLE II
SEA STATE CONDITIONS FOR THE NORTH SEA SITE

	H_s	T_p	Probability	Occurrence/year
1	0.64	6.06	13.1	1145
2	0.73	6.13	8	698.2
3	0.77	6.17	2.1	186.2
4	0.8	6.19	0.3	27.9
5	1.26	6.55	5.8	512
6	1.43	6.68	17.3	1517.4
7	1.56	6.78	13.2	1154.3
8	1.63	6.83	3.9	344.4
9	1.66	6.86	0.6	55.9
10	1.69	6.88	0.1	9.3
11	2.22	7.28	1.9	167.6
12	2.37	7.4	9.5	828.5
13	2.51	7.5	8.5	744.7
14	2.58	7.56	2.6	223.4
15	2.61	7.58	0.3	27.9
16	3.21	8.05	0.6	55.9
17	3.35	8.16	3.9	344.4
18	3.48	8.26	3.5	307.2
19	3.55	8.32	1	83.8
20	3.59	8.35	0.1	9.3
21	4.21	8.85	0.2	18.6
22	4.35	8.96	1.4	121.09
23	4.47	9.06	1.1	93.1
24	4.54	9.11	0.2	18.6
25	5.22	9.68	0.1	9.3
26	5.36	9.8	0.4	37.2
27	5.47	9.89	0.2	18.6

TABLE III
SEA STATE CONDITIONS FOR THE NORWAY SITE

	H_s	T_p	Probability	Occurrence/year
1	0.67	9.48	3.3	282.2
2	0.7	9.51	3.9	335
3	0.73	9.55	1.1	92.7
4	0.77	9.59	0.1	9.5
5	1.5	10.3	7.2	615.9
6	1.54	10.33	12.5	1070.4
7	1.58	10.36	5.6	479.2
8	1.62	10.39	0.9	79.2
9	1.65	10.41	0.1	5.4
10	2.42	10.94	4.4	374.7
11	2.46	10.96	12.1	1035.5
12	2.51	10.99	9.4	806.9
13	2.56	11.02	2.5	212.9
14	2.59	11.04	0.2	21.3
15	3.35	11.46	1.1	93.7
16	3.4	11.48	5.3	541.4
17	3.46	11.51	8.2	699.5
18	3.52	11.54	3.8	327.5
19	3.56	11.56	0.6	49.4
20	4.3	11.91	0.1	10.1
21	4.34	11.93	1.1	92.2
22	4.41	11.96	3.8	326.4
23	4.48	11.99	3.7	315.4
24	4.53	12.01	0.9	479.8
25	4.56	12.03	0.1	6.4
26	5.29	12.33	0.1	8.6
27	5.36	12.36	0.9	78.9
28	5.43	12.39	2.2	185.5
29	5.5	12.42	1.1	91.7
30	5.54	12.44	0.1	11.3
31	6.3	12.73	0.1	9.3
32	6.38	12.76	0.7	62.4
33	6.46	12.79	0.8	72
34	6.52	12.81	0.2	15.6
35	7.33	13.11	0.1	11
36	7.42	13.14	0.4	36
37	7.49	13.16	0.2	16.3
38	8.37	13.46	0.1	10.4
39	8.46	13.49	0.1	12.1
40	9.42	13.81	0.1	5.9

frequency-domain model. The model is based on linear wave theory, where wave height is assumed to be much smaller than wave length and water depth, and oscillations are assumed to be small. In this case, waves are represented as harmonic oscillations of different wave height and frequency, which can be linearly superposed to represent an irregular sea. For each sea state the relation of wave amplitude to frequency is defined by a Bretschneider spectrum, where 150 frequencies (ω_k) from 0 to 3 rad/s in 0.02 steps are analysed.

Under these assumptions, the equation of motion of a WEC can be written as in (1), where the main forces affecting the motion will be the wave excitation force $\mathbf{F}_e$, the PTO-force $\mathbf{F}_{PTO}$, the WEC inertia $\mathbf{M}$, the radiation force composed of an added mass $\mathbf{M}_{rad}$ and an added damping $\mathbf{C}_{rad}$ terms, and the hydrostatic force represented by a stiffness term $\mathbf{K}_H$ following Archimedes principle. An additional damping term $\mathbf{C}_{loss}$ is included to represent friction losses as in [2]. The stiffness value from the mooring lines is neglected, because it is considered to be much smaller than the hydrostatic stiffness value.

$$\begin{aligned}\hat{\mathbf{F}}_e + \hat{\mathbf{F}}_{PTO} =&[-\omega^2(\mathbf{M}+\mathbf{M}_{rad}) + i\omega(\mathbf{C}_{rad}+\mathbf{C}_{loss}) \\ &+ \mathbf{K}_H]\hat{\mathbf{X}}(\omega_k)\end{aligned} \tag{1}$$

An idealised optimal control strategy is assumed, which sets the mass, damping and stiffness terms composing the PTO force to match the impedance $\mathbf{Z}$, as defined in (2), at the energy period $T_e = 2\pi/\omega_e$. Here $\hat{\mathbf{U}}$ represents a vector of complex amplitudes of the oscillation velocity in six degrees of freedom, and $\hat{\mathbf{X}}$ is the corresponding vector of complex amplitudes of oscillation.

$$\hat{\mathbf{F}}_e = \mathbf{Z}\hat{\mathbf{U}} = \mathbf{Z}i\omega\hat{\mathbf{X}} \tag{2}$$

Then the PTO force is defined by the complex conjugate of the impedance $\mathbf{Z}^*$ as shown in (3).

$$\begin{aligned}\hat{\mathbf{F}}_{PTO} &= -\mathbf{Z}^*\hat{U} = -\mathbf{Z}^*i\omega\hat{\mathbf{X}} \\ &= [-\omega^2(\mathbf{M}+\mathbf{M}_{rad}(\omega_e)) - i\omega(\mathbf{C}_{rad}(\omega_e)+\mathbf{C}_{loss}) \\ &\quad + \mathbf{K}_H]\hat{\mathbf{X}}\end{aligned} \tag{3}$$

The time series of the PTO force $F_{PTO_{s,q}}(t)$ can then be obtained for each sea state s and set q of random phase shifts $\psi_{s,k,q}$ from the superposition of the single harmonic force representations at each frequency ω_k.

$$\begin{aligned}F_{PTO_{s,q}}(t) = \sum_{k=1}^{N} \Big(&\Big|\hat{F}_{PTO_s}(\omega_k)\Big| \cos(\omega_k t + \psi_{s,k,q} + \\ &\angle\hat{F}_{PTO_s}(\omega_k)\Big)\end{aligned} \tag{4}$$

PTO stroke constraints are considered here by setting the PTO force to 0 when the maximum stroke (5m) is exceeded, since it is assumed that the end stops will be taking all the load in this situation. PTO rating constraints are assumed here to calculate the average annual power as in [8], but are considered to have no effect on the PTO-force time series.

An example of the PTO force time series for a heaving cylinder in the North Sea can be seen in Figure 3, where sea states are numbered according to Table II.

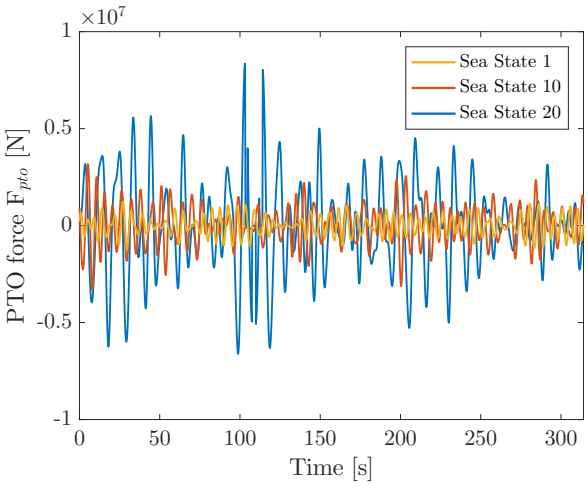

Fig. 3. PTO force time series for a heaving cylinder in the North Sea for three different sea states.

C. Fatigue Damage Analysis

In total, 10 PTO time force series were generated for each case. Descriptions of these 12 cases are in Table VI.

TABLE IV
DEFINITION OF CASES

Case	Location	Motion	Shape
1	North Sea	Heave	Cylinder
2	North Sea	Heave	Sphere
3	North Sea	Heave	Barge
4	North Sea	Surge	Cylinder
5	North Sea	Surge	Sphere
6	North Sea	Surge	Barge
7	Norway	Heave	Cylinder
8	Norway	Heave	Sphere
9	Norway	Heave	Barge
10	Norway	Surge	Cylinder
11	Norway	Surge	Sphere
12	Norway	Surge	Barge

For our analysis, we focused on the fatigue failure of the rod weld connecting the floater to the PTO. Fatigue failures are speculated to be a common failure mode in WECs, occurring at welded joints or corroded bolts [5]. Furthermore, this type of failure has high technical and economic consequence, with the failure of the weld causing complete failure of the device and costly repair via re-welding either at sea or in port.

We used DNV Standards on Fatigue Design of Offshore Steel Structures [11], specifically S-N Curve D in Table A5 for stress perpendicular to the weld, with a traverse splice in rolled sections. This curve assumes the weld is subject to seawater and has cathodic protection. Paired with this curve, we analyzed the time-series with WAFO's [12] Rainflow Counting algorithm to quantify the stress cycle time series data.

We binned the counted stress cycles by their amplitudes in 20 bins, as suggested by Wægter [13]. We then used Palmgren-Miner's rule to estimate the weld

fatigue caused by each binned stress range for each sea state. That is, for each bin, we divide the number of cycles in that bin by the number of cycles to failure for the given stress range. The cycles to failure, or the component capacity against fatigue, is determined by Eq. 5.

$$n_c(s) = a_D s^{-m} \tag{5}$$

where $n_c(s)$ is the number of stress ranges (or the number of cycles) in a given amplitude, a_D is the intercept parameter of the S-N curve, s is the stress range (double the amplitude) in MPa, and m is the slope of the S-N Curve. These S-N Curve and Rainflow Counting details are included in Table V.

TABLE V
FATIGUE ANALYSIS DETAILS

Parameter	Value
a_D	11.764e6
m	3
Rod Diameter (m)	6
Number of Force Range Bins	20
Lifespan (years)	20

The results for each sea state are then multiplied by the expected number of times they occur during the lifetime of the structure to obtain a measure of the total fatigue damage. We repeat this for each case with 10 PTO force time series to gain an understanding of the variation in fatigue DEL.

III. RESULTS & DISCUSSION

In this section, we separate our results by whether the WEC is heaving or surging and by its location (North Sea and Norway).

Figures 4 and 5 represent the two motions of oscillation in the North Sea. Across the site-specific sea states, heave cases have lower DELs, while surge cases have higher DELs. Both heave and surge motions show similar patterns of DELs. For instance, DELs in sea states 22, 27, 19 and 13 are the greatest in both heave and surge motions. This is attributed to the combination of relatively high values for wave height, wave period, and probability of occurrence.

When considering the DELs across shapes, the sphere cases have higher DELs in the heave cases at high sea states, but the cylinder and barge cases have higher DELs at lower sea states in heave cases. In the surge cases, the cylinder and barge cases have consistently higher DELs than the sphere cases.

Figures 6 and 7 depict the the two motions of oscillation at the Norway site. Across heave and surge motions, the barge and cylinder cases show fairly consistent DELs regardless of whether the WEC is heaving or surging. The sphere cases, unlike at the North Sea site, show higher DELs than in the heave case, and lower DELs in the surge case.

The highest DELs achieved are in the surging cases in the North Sea, coinciding with the high probability of higher energetic sea states.

Overall the performance of the different shapes, can be analysed considering also their annual average power production, shown in Table VI. Results indicate that the barge shape has the highest DELs across most cases and sea states, although it also achieves the highest power production in Norway in both heave and surge, and the second highest in the North Sea, when compared to the other shapes. The reason for this, can be the much higher submerged volume of the barge, which is approximately two times the submerged volume of the sphere and more than six times the submerged volume of the cylinder. In contrast, the sphere shape performs the best, but it seems to be highly sensitive to whether it is moving in heave or surge. It has the lowest DELs across most cases and sea states, and produces the highest power in the North Sea in both heave and surge, and performs similarly to the barge in Norway. To be able to compare the suitability of different shapes more fairly, these results point to the fact that, different shapes of equal submerged volume should be analysed additionally, to eliminate the effect that this might have on both fatigue and power performance results.

TABLE VI
POWER PRODUCTION ACROSS CASES

Case	Location	Motion	Shape	Average Power [W]
1	North Sea	Heave	Cylinder	143,209.838
2	North Sea	Heave	Sphere	157,655.814
3	North Sea	Heave	Barge	144,106.806
4	North Sea	Surge	Cylinder	28,580.939
5	North Sea	Surge	Sphere	34,637.542
6	North Sea	Surge	Barge	30,268.821
7	Norway	Heave	Cylinder	536,946.397
8	Norway	Heave	Sphere	592,297.634
9	Norway	Heave	Barge	602,030.775
10	Norway	Surge	Cylinder	427,543.969
11	Norway	Surge	Sphere	524,400.879
12	Norway	Surge	Barge	527,765.532

IV. CONCLUSIONS

In this study, we explore the relationship between WEC floater hull geometry and PTO reliability. We analyse 12 cases in total, across two locations (North Sea and Norway), two modes of motion (heave and surge), and three shapes (barge, cylinder, and sphere). Based on these conditions, we measure the damage equivalent load (DEL) on the rod weld connecting the floater to the PTO.

Results indicate a clear dependence of DELs on location, oscillation direction, and shape. Therefore, it is critical to consider these parameters in the early design of WECs. Moreover, this study makes the case for incorporating reliability objectives into early design simultaneously with power production and cost, rather than secondary to them. Incorporating reliability in conjunction with power production and cost objectives will enable developers and researchers to design more optimal WECs, advancing the techno-economic feasibility of this technology.

In future work, we plan to expand upon the methods included in this study to use a more detailed PTO model. More importantly, this study will be used as the basis for future reliability-based design optimization

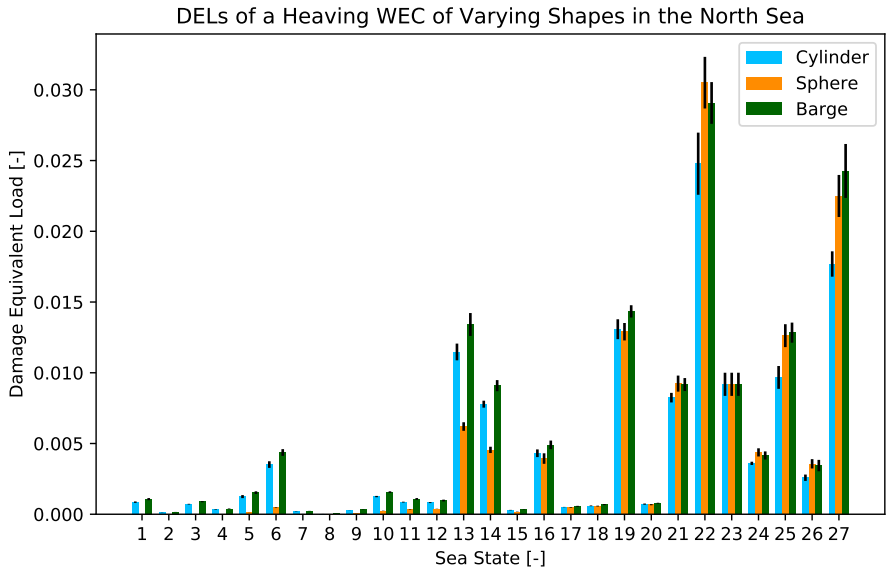

Fig. 4. Damage equivalent loads across sea states for a WEC of varying shapes heaving in the North Sea

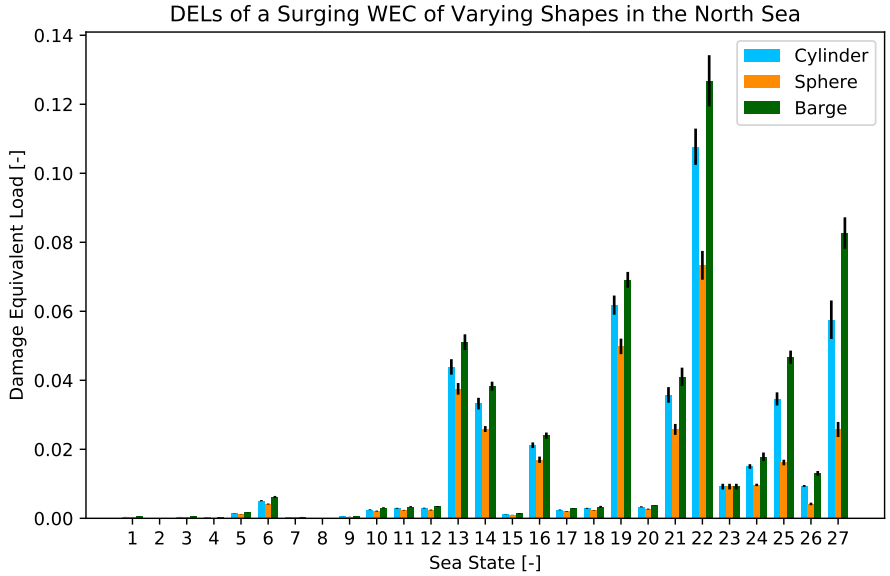

Fig. 5. Damage equivalent loads across sea states for a WEC of varying shapes surging in the North Sea

work that optimizes WEC floater hull geometry to improve PTO reliability, power production, and cost.

References

[1] R. Coe, Y.-H. Yu, J. van Rij, R. G. Coe, Y.-H. Yu, and J. van Rij, "A Survey of WEC Reliability, Survival and Design Practices," *Energies*, vol. 11, no. 1, p. 4, dec 2017. [Online]. Available: http://www.mdpi.com/1996-1073/11/1/4

[2] A. McCabe, "Constrained optimization of the shape of a wave energy collector by genetic algorithm," *Renew. Energy*, vol. 51, pp. 274–284, mar 2013. [Online]. Available: http://www.sciencedirect.com/science/article/pii/S0960148112006258

[3] M. Blanco, P. Moreno-Torres, M. Lafoz, and D. Ramírez, "Design parameter analysis of point absorber WEC via an evolutionary-algorithm-based dimensioning tool," *Energies*, vol. 8, no. 10, pp. 11 203–11 233, 2015.

[4] A. Babarit and A. H. Clément, "Shape optimisation of the SEAREV wave energy converter," *9th World Renew. Energy Congr.*, 2006.

[5] S. Ambühl, M. Kramer, and J. D. Sørensen, "Reliability-Based Structural Optimization of Wave Energy Converters," *Energies*, vol. 7, pp. 8178–8200, 2014. [Online]. Available: www.mdpi.com/journal/energies

[6] P. J. B. F. N. Beirão and C. M. dos Santos Pereira Malça, "Design and analysis of buoy geometries for a wave energy converter," *Int. J. Energy Environ. Eng.*, vol. 5, no. 2-3, p. 91, jul

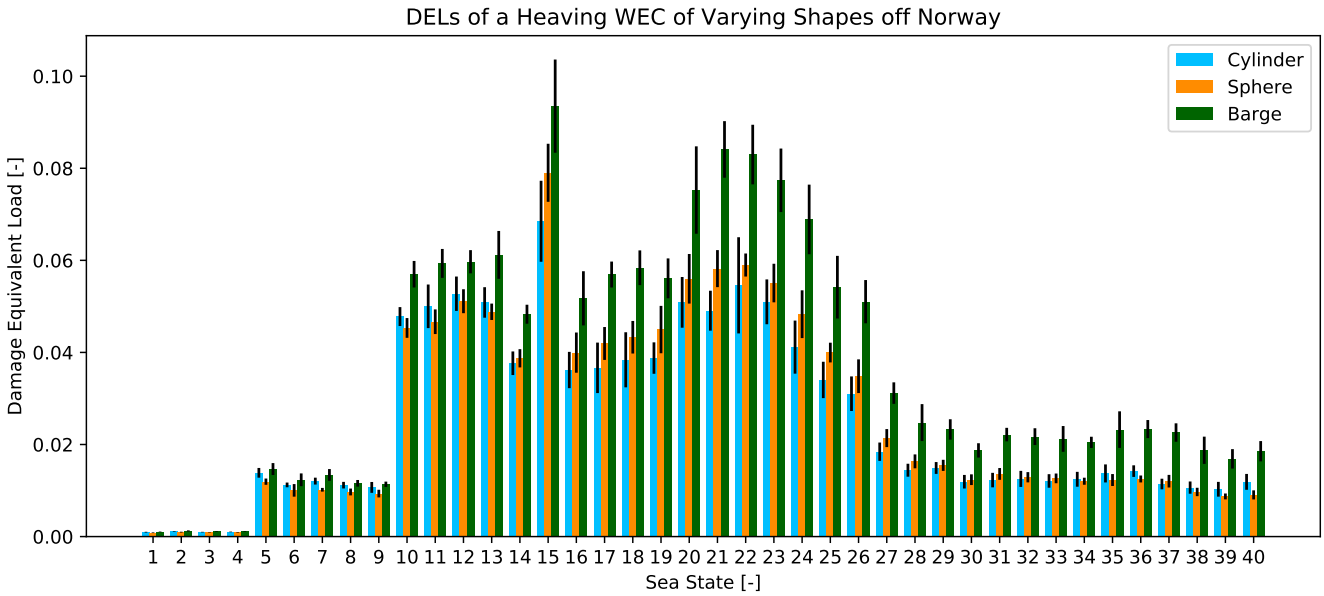

Fig. 6. Damage equivalent loads across sea states for a WEC of varying shapes heaving off Norway

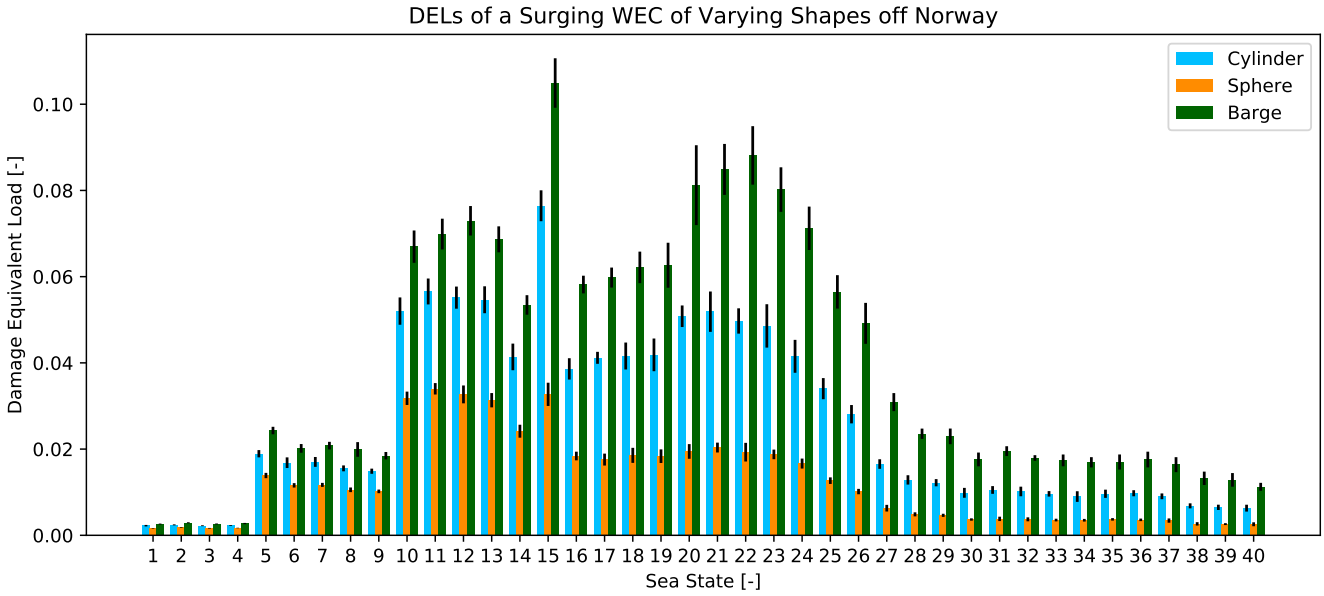

Fig. 7. Damage equivalent loads across sea states for a WEC of varying shapes surging off Norway

2014. [Online]. Available: http://link.springer.com/10.1007/s40095-014-0091-7

[7] J. van Rij, Y.-H. Yu, K. Edwards, and M. Mekhiche, "Ocean power technology design optimization," *Int. J. Mar. Energy*, vol. 20, pp. 97–108, dec 2017. [Online]. Available: https://www.sciencedirect.com/science/article/pii/S2214166917300656

[8] A. Garcia-Teruel and D. Forehand, "Optimal wave energy converter geometry for different modes of motion," in *Adv. Renew. Energies Offshore Proc. 3rd Int. Conf. Renew. Energies Offshore (RENEW 2018)*, Lisbon, 2018, pp. 299–305.

[9] M. Sojo Armentia and G. Auer, "MARINA Platform Final Summary Report," Tech. Rep., 2014.

[10] L. Li, Z. Gao, and T. Moan, "Joint Environmental Data at Five European Offshore Sites for Design of Combined Wind and Wave Energy Devices," *Vol. 8 Ocean Renew. Energy*, vol. 8, no. 7491, p. V008T09A006, 2013. [Online]. Available: http://www.scopus.com/inward/record.url?eid=2-s2.0-84893074848{\&}partnerID=tZOtx3y1

[11] DNV, "RP-C203- Fatigue design of offshore steel structures," *Recomm. Pract. DNV-RPC203*, no. October, p. 126, 2014. [Online]. Available: ftp://128.84.241.91/tmp/MSE-4020/Fatigue-Design-Offshore.pdf

[12] The WAFO Group, "WAFOa Matlab toolbox for analysis of random waves and loads," Lund University, Lund, Sweden, Tech. Rep. March, 2011. [Online]. Available: http://www.maths.lth.se/matstat/wafo/documentation/wafoiso.ps

[13] J. Waegter, "Stress range histories and Rain Flow counting," 2009, no. June, pp. 1–13.